18TH WORLD CONFERENCE ON EARTHQUAKE ENGINEERING
WCEE2024
MILAN

MILAN, ITALY
30TH JUNE - 5TH JULY 2024

www.wcee2024.it

VERTICAL-ROCKING ISOLATION: FULL-SCALE SHAKING TABLE TESTS AND MODELING OF A 3000-LITER STORAGE TANK

S. I. Reyes[1], M. F. Vassiliou[1], J. L. Almazán[2,3], N. F. Tapia[2], J. I. Colombo[4] & J. C. de la Llera[2]

[1] Chair of Seismic Design and Analysis, Institute of Structural Engineering (IBK), Swiss Federal Institute of Technology (ETH) Zürich, Switzerland.

[2] Department of Structural and Geotechnical Engineering, Pontificia Universidad Católica de Chile, Chile.

[3] Centro Nacional de Excelencia para la industria de la madera (CENAMAD), Pontificia Universidad Católica de Chile, Chile

[4] Department of Civil Engineering, Universidad Diego Portales, Chile

Abstract: *This paper presents the experimental and numerical validation of a Vertical-Rocking Isolation (VRI) system. The system uses vertically flexible and laterally rigid isolation devices to enable rocking motion isolation of a liquid storage tank. The evaluation involves 1-D shaking table tests conducted on a full-scale 3000-liter legged tank. The isolation system has four ISO3D-2G devices placed on each leg of the tank, and uses high-damping natural rubber in compression for restoring forces and energy dissipation. The tests employ 17 ground motion inputs for system validation. Measured variables include lateral acceleration and displacement of the tank, as well as vertical and rotational motions of the isolation interface. For motions with Peak Ground Acceleration (PGA) values between 0.3 and 0.8 g, the maximum displacement at the top of the tank remains below 13 cm (4% of total height), with total accelerations close to 0.3 g without any observable damage. Also, a simplified lumped-mass model is used for the numerical representation of the system, and is used to predict mean maximum values with errors smaller than 10% and 21% for displacements and accelerations, respectively. These results demonstrate that the behavior of vertical-rocking isolated structures can be reasonably predicted using a simplified model, suggesting the possibility of developing simple design guidelines and equations for the VRI system even in the presence of liquids.*

1. Introduction

Seismic isolation is a widely applied method for protecting structures against earthquakes (Wada *et al.*, 2008; Makris, 2019; Ramirez *et al.*, 2020; Zhang and Zhou, 2023). The traditional way to achieve it is by placing a horizontally flexible interface below the structure to decouple it from the ground. This elongates the fundamental period of the structure to values where lower spectral accelerations are expected. The most common ways to materialize this behavior are using elastomeric bearings, sliding plates, roller or ball bearings, sleeved piles, cable suspension systems, air cushions, and coil springs (Buckle and Mayes, 1990). Three-dimensional seismic isolation concepts that would protect from vertical ground excitations have also been explored. This is generally achieved by including an additional device to provide the vertical isolation, which is placed in series to the one that provides the horizontal isolation. Some examples are the use of Frictional Pendulum or laminated rubber bearings supported on different vertically flexible systems, or on vertical helical springs in viscous fluid (Makris and Constantinou, 1992).

Including this additional vertical flexibility creates an additional vertical-rocking mode that is generally suppressed, given that it is a not desired mode when protecting buildings. However, some individual critical

components from industrial facilities and essential services that have shown a poor performance on earthquakes (McKevitt, Timler and Lo, 1995) may allow this flexible rocking mode and this can be an effective mechanism to better fit the specific requirements of lighter structures and equipment of industrial facilities cost-efficiently. Such rocking systems have been used to protect slender electrical substation equipment where because of their shape, horizontal base isolation is not the most effective way of protection. Wire ropes devices (Alessandri *et al.*, 2015) and friction spring dampers (Riley *et al.*, 2006) are typically used for this purpose; however, they are anchored to the structure and the ground and when they dynamically reach their maximum displacement in tension, they get locked and transmit impact forces to the structure, which may lead to significant damage and even collapse. This vertical restraining is used due to an inherent fear of collapse by overturning; however, it is well known that restraining this behavior leads to an increase in the internal forces on the elements, which are also transmitted to the foundations. Notwithstanding this, when possible (i.e., when the slenderness of the structure allows it), it is recommended to allow uplift since it works as a mechanical fuse and limits the design forces on the superstructure (Housner, 1963; Kelly, 2008; Reggiani Manzo and Vassiliou, 2019; Wang and Ishihara, 2020; Elmorsy and Vassiliou, 2023).

Legged thin-walled liquid storage tanks are interesting candidate structures to protect with a rocking isolation system. The main reason is that their liquid content does not fully contribute to the system's rotational inertia, which is beneficial for rocking motions in terms of reducing the base shear (Makris, 2014). Storage tanks have shown a deficient seismic performance during recent earthquakes, generating significant economic losses worldwide (Rosewitz and Kahanek, 2014; Daniell and Schäfer, 2018; Moreno *et al.*, 2023; Tapia *et al.*, 2023). Thus, it is interesting to apply a VRI system with the possibility of uplifting to these types of structures, which, besides reducing the lateral demand, also helps in isolating from the vertical component of the earthquake (Almazan and Reyes, 2021).

This research aims to experimentally evaluate the dynamic performance of a Vertical-Rocking Isolation (VRI) system with uplift allowed on a 3,000-liter legged storage tank, and to validate a numerical model to represent the whole system's behavior. The isolation system comprises four ISO3D-2G devices, which use unbonded rubber to provide restoring and dissipative forces. The whole device can only take compression. However, a compressive deformation of the device causes part of the rubber (i.e. the central annular rubber) to be in compression and part of the rubber (i.e. the rubber bands) to be in tension. This system is expected to be a relatively low-cost solution due to the unbounded condition of the rubber (no vulcanization or bonding process is needed) and the absence of anchors to the foundation. The tests were conducted on a 1-D shaking table at the Structural Engineering Laboratory of Pontificia Universidad Católica de Chile.

This paper starts by briefly presenting the fundamental aspects of a vertical rocking isolation system with its theoretical background. Then, the complete experimental campaign is described, followed by a section with the system identification of the structure performed with the white noise inputs. A simplified rigid-body model is developed to represent the behavior of the tank and isolators. Finally, the results and observations of the tests are presented, as well as the performance of the numerical model to estimate the measured peak responses.

2. Description of the Vertical-Rocking Isolation System

In a VRI system, the desired flexible degrees of freedom at the isolation interface are two: rotation and vertical translation (Reyes and Almazán, 2019, 2020; Reyes *et al.*, 2020; Reyes *et al.*, 2022). Lateral translation and torsional rotation at the isolation interface are restricted, and the isolation effects should be generated entirely by the rotation at the base of the structure. In addition, for large seismic demand, the system allows for the uplifting of the isolation interface to limit the design forces transmitted to the structure . Allowing for the uplifting of the isolation interface also enables easy equipment relocation inside the facility (there is no need to anchor the structure to the floor), and the forces transmitted to the foundations are reduced, thus lowering their dimension and cost.

Figure 1 a shows a planar block isolated with a pair of Vertical-Rocking Isolators (VRIs), which is assumed to be linear and have a stiffness k. Figure 1b and Figure 1c present the two vibration modes, assuming small rotations and no uplift. In the rocking mode, an Instantaneous Center of Rotation (ICR) can be identified, and the system's kinematics can be defined by rotations about this point when the structure is considered a rigid

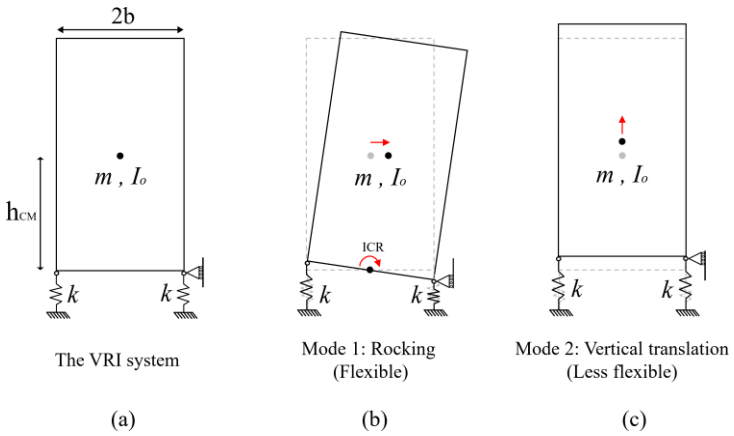

Figure 1. : (a) The VRI system, (b) flexible first rocking mode, (c) less flexible vertical mode. (Note: The springs cannot take tension. Therefore Mode 1 and Mode 2 correspond to decompression of the springs; not tension. Their initial compression is caused by the weight).

body. For linear analyses, during a rocking motion (i.e., Figure 1b) the ICR remains at the same distance from the two springs (since the stiffnesses of both springs are equal and constant). The corresponding eigen-periods T_1 and T_2 of the rocking mode and vertical mode, respectively, are:

$$T_1 = 2\pi\sqrt{\frac{I_o + mh_{CM}^2}{2kb^2 - mgh_{CM}^2}} \quad (1)$$

$$T_2 = 2\pi\sqrt{\frac{m}{2k}} \quad (2)$$

where I_o is the rotational inertia of the block with respect to its Center of Mass (CM), m is the mass of the block, h is the height of the CM with respect to the rocking axis, g is the vertical acceleration of gravity, b is the half base of the block, and k is the vertical stiffness of the linear springs. In linear analyses, the horizontal ground motion only excites the first mode. Nonlinear behavior comes from uplift or nonlinear force-deformation relationship of the VRIs, and results in a more complex behavior with a coupling of modes and a variable position of the ICR given the variable tangent stiffness of the nonlinear devices (i.e., a variable value of b).

3. Description of the experimental program

The tested structure corresponds to a typical 3,000-liter storage tank supported on 4 ISO3D-2G devices, welded to the four legs of the tank. The tank was placed on a 1-D shaking table installed at the Laboratory of the Department of Structural and Geotechnical Engineering of the Pontificia Universidad Católica de Chile. Therefore, the behavior under 3D excitation is not studied in this work. For the 4 tons payload, the maximum velocity and acceleration of the table is 200 mm/s and 0.5g, respectively; the maximum stroke is ± 500 mm.

A 2 mm neoprene sheet was placed below the devices to increase friction with the table and avoid sliding. The liquid used in the tests was water (similar density to wine), and a baffle was placed in the neck to minimize sloshing. This small free-surface condition is also consistent with practice in the winemaking process (i.e., tanks fully filled with wine). The total mass of the steel tank (without water inside) *is* m_{tank}*=250 kg*, and its CM is at the height of 1,573 mm with respect to the rotation point of the devices.

Figure 2 presents images of the setup, the dimensions, and the instrumentation considered: (i) three linear variable differential transformers (LVDTs) to measure the absolute lateral displacement at the isolation level (D_{legs}), close to the midheight (D_{middle}), and at the top of the structure (D_{top}); (ii) an LVDT to measure the absolute lateral displacement of the table; (iii) four LVDTs to measure the vertical displacement at the top of the devices with respect to the shaking table, (iv) two LVDTs to measure the vertical uplift from the table of two diagonally opposite devices; and (v) three piezoelectric accelerometers measuring the horizontal acceleration of the tank at a different height and the horizontal acceleration of the shaking table (all the accelerometers were set up in the direction of the applied motion). All sampling frequencies were set to 200 Hz for the seismic inputs.

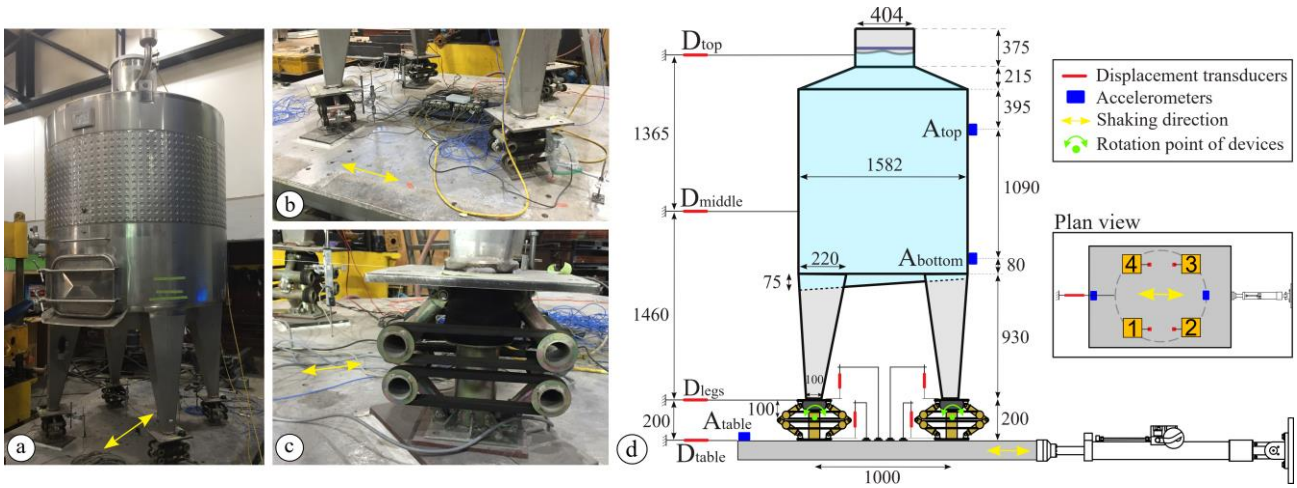

Figure 2. Experimental setup for the tests: (a) general view of the tank on the shaking table, (b) supporting devices, (c) close up to an ISO3D-2G device, and (d) instrumentation and dimensions (in mm) of the test setup.

The structure was first excited with three White-noise (W-N) records scaled to three different intensities for system identification, and after 45 days, it was subjected to 17 consecutive earthquake excitations (within a time frame of about 8 hours). To keep the manuscript concise, only the results from the earthquake excitations are presented and analyzed herein. System identification results can be found elsewhere (Reyes *et al.*, 2022). Both artificial and natural excitations recorded from the 2010 Mw 8.8 Maule Earthquake were used. These records were also used elsewhere (Colombo and Almazán, 2017). The target spectrum of the artificial records corresponded to the Chilean code spectrum for seismically isolated structures for 5% damping, soil type I, and seismic zone III. Additionally, one of the records corresponded to a harmonic sinusoidal input with a frequency of 1Hz.

Table 1 presents all input records with their respective identifier number, names, scaling, and measured peak acceleration, velocity, and displacement. All acceleration records that were used as input for the table were filtered using a low-pass (LP) filter with a cut-off frequency of 40 Hz, and a high-pass (HP) filter with a cut-off frequency of 0.1 Hz. The controller integrates this acceleration signal to produce a displacement signal which afterward passes through a HP filter with a cut-off frequency of 0.2 Hz. Since the tested structure was full-scale, no time scaling was necessary. More information about the test and ground motions can be found in (Reyes *et al.*, 2022).

Table 1. Ground motion information (as reproduced by the shake table).

# ID	Record name	Scaling	PGA [g]	PGV [mm/s]	PGD [mm]
1	Talca	50%	0.287	202	39.2
2	Talca	75%	0.435	307	59.9
3	Talca	100%	0.589	408	77.4
4	Talca	120%	0.783	464	84.1
5	Harmonic (1 Hz)	65%	0.307	191	25.2
6	Curicó	75%	0.303	125	24.7
7	Curicó	100%	0.419	152	31.9
8	Curicó	120%	0.527	182	36.5
9	Synthetic A	75%	0.431	186	31.3
10	Synthetic A	100%	0.499	260	42.5
11	Synthetic A	120%	0.566	314	51.9
12	Synthetic B	75%	0.431	187	32.6
13	Synthetic B	100%	0.526	241	43.6
14	Synthetic B	120%	0.560	283	52.0
15	Synthetic C	75%	0.454	204	29.7
16	Synthetic C	100%	0.488	276	39.7
17	Synthetic C	120%	0.591	307	47.8

4. Simplified modeling of the VRI system

1.1. Equations of motion

Figure 3 shows a simplified 3 degree-of-freedom (DOF) representation of the system. Other studies have used similar approaches for seismically isolated structures (Olivares, de la Llera and Poulos, 2020). The simplified model assumes that the superstructure behaves as a rigid body and can be modeled as a lumped inertial mass m_i, with a given rotational inertia I_i, at a representative height h_i, for each global direction i=x, y, z. The equivalent properties of the system (i.e., seismic mass, rotational inertia, and height) in each principal direction can differ given they need to be chosen according to the sloshing dynamic theory. This is explained in detail in a separate subsection. Thus, the equation that governs the motion of the structure, assuming linear kinematics, can be expressed as a 6 DOF system as follows (Reyes and Almazán, 2020):

$$\mathbf{M}\ddot{\mathbf{q}}(t)+\mathbf{K}_{\mathbf{geo}}\mathbf{q}(t)+\mathbf{L}^{\mathbf{T}}\mathbf{F}_{\mathbf{NL}}(t)=\mathbf{W}-\mathbf{S}\ddot{\mathbf{U}}_{\mathbf{g}}(t) \tag{3}$$

$$\mathbf{q}(t)_{(6\times1)}=\begin{bmatrix}u_x(t) & u_y(t) & u_z(t) & \theta_x(t) & \theta_y(t) & \theta_z(t)\end{bmatrix}^T \tag{4}$$

$$\mathbf{M}_{(6\times6)}=\begin{bmatrix} m_x & 0 & 0 & 0 & m_xh_x & 0 \\ 0 & m_y & 0 & -m_yh_y & 0 & 0 \\ 0 & 0 & m_z & 0 & 0 & 0 \\ 0 & -m_yh_y & 0 & m_xh_x^2+I_y & 0 & 0 \\ m_xh_x & 0 & 0 & 0 & m_yh_y^2+I_x & 0 \\ 0 & 0 & 0 & 0 & 0 & I_z \end{bmatrix} \tag{5}$$

$$\mathbf{K}_{\mathbf{geo}(6\times6)}=\begin{bmatrix} 0 & 0 & 0 & 0 & 0 & 0 \\ 0 & 0 & 0 & 0 & 0 & 0 \\ 0 & 0 & 0 & 0 & 0 & 0 \\ 0 & 0 & 0 & -m_zh_z\left(g+\ddot{U}_{gz}(t)\right) & 0 & 0 \\ 0 & 0 & 0 & 0 & -m_zh_z\left(g+\ddot{U}_{gz}(t)\right) & 0 \\ 0 & 0 & 0 & 0 & 0 & 0 \end{bmatrix} \tag{6}$$

$$\mathbf{F}_{\mathbf{NL}}(t)_{(3n\times1)}=\begin{bmatrix}F_x^{(1)}(t) & F_y^{(1)}(t) & F_z^{(1)}(t) & \cdots & F_x^{(n)}(t) & F_y^{(n)}(t) & F_z^{(n)}(t)\end{bmatrix}^T \tag{7}$$

$$\mathbf{L}_{(3n\times6)}=\begin{bmatrix} L_{(3\times6)}^{(1)} \\ \vdots \\ L_{(3\times6)}^{(n)} \end{bmatrix} \tag{8}$$

$$\mathbf{W}_{(6\times1)}=\begin{bmatrix}0 & 0 & -m_zg & 0 & 0 & 0\end{bmatrix}^T \tag{9}$$

$$\ddot{\mathbf{U}}_{\mathbf{g}}(t)_{(3\times1)}=\begin{bmatrix}\ddot{u}_{gx}(t) & \ddot{u}_{gy}(t) & \ddot{u}_{gz}(t)\end{bmatrix}^T \tag{10}$$

$$\mathbf{S}_{(6\times3)}=\begin{bmatrix} m_x & 0 & 0 \\ 0 & m_y & 0 \\ 0 & 0 & m_z \\ 0 & -m_yh_y & 0 \\ m_xh_y & 0 & 0 \\ 0 & 0 & 0 \end{bmatrix} \tag{11}$$

where **q**(t) is the vector of the six DOF located below the equivalent mass at the isolation interface (as shown in Figure 3a); matrices **M** and $\mathbf{K_{geo}}$ are the mass and geometric stiffness, respectively; **W is** the self-weight vector and g the acceleration of gravity. M_i, h_i, and I_i are the mass, height, and rotational inertia of the equivalent

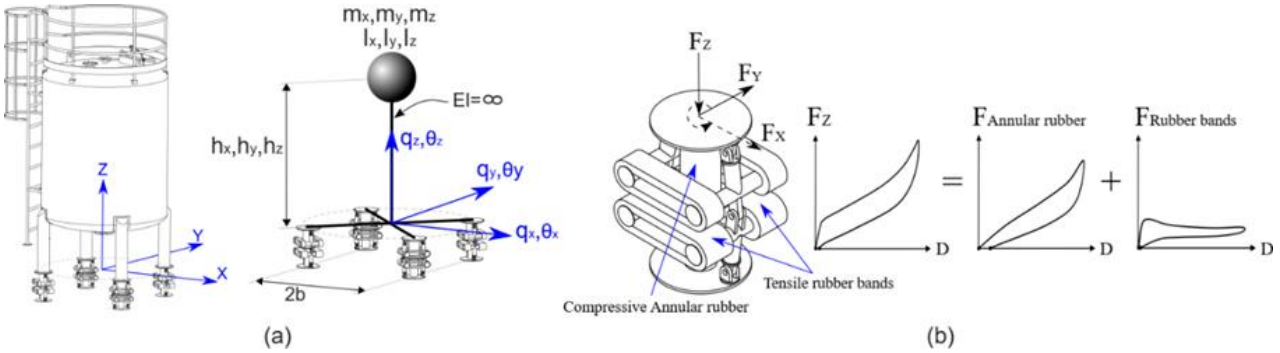

Figure 3. (a)Tank supported on four ISO3D-2G devices and simplified lumped-mass model, (b) ISO3D-2G device with the three DOF considered in the modeling, and the schematic contribution of the compressive annular rubber and tensile rubber bands to the vertical force-deformation relationship.

lumped mass in a given direction *i=x, y, z,* respectively. $\mathbf{F_{NL}}(t)$ is the vector that contains the local nonlinear forces of the *n* devices involved in the system, and **L** is a kinematic transformation matrix from local forces to global coordinates. $\ddot{\mathbf{U}}_g(t)$ is the ground acceleration vector where rotational accelerations are neglected, and **S** is the matrix that relates each component of the ground motion with the specific excited DOFs. All these expressions were obtained by formulating the Euler-Lagrange equations. Notice that the geometric stiffness matrix involves only first-order P-delta effects due to the constant acceleration of gravity *g* and the additional vertical acceleration of the ground since the restoring forces are provided only by the nonlinear term $\mathbf{L}^T\mathbf{F}_{NL}(t)$.

1.2. Equivalent properties of the system's center of mass

The tank (i.e., steel part) can be considered a rigid body with its respective mass and inertia; however, the liquid inside is modeled with equivalent properties that are defined accordingly for the liquid sloshing dynamics theory (Raouf, 2005). Thus, the mass needs to be defined according to an impulsive and convective mass. In the literature, there are widely-accepted tabulated values for the impulsive and convective parameters based on the aspect ratio *H/r* of a flat cylindrical tank of radius *r* and filled with water up to a height *H* subject to lateral acceleration. Given that the water in the tank has a minimal free surface, its behavior is governed by the impulsive mass (Malhotra, Wenk and Wieland, 2000). Recent experimental studies (Moosapoor, Yousefi and Goudarzi, 2019; Goudarzi, Moosapoor and Nikoomanesh, 2020) have validated this statement for cylindrical tanks with an aspect ratio similar to the one used in this study. Nevertheless, it should be noted that some of the assumptions made by Malhotra, Wenk and Wieland (2000) deviate from the experimental conditions of the tests: i) the tank has legs, ii) rocking motions are involved, iii) convective modes are suppressed, and iv) the radius of the free surface is considerably smaller than the main body. Despite these deviations, structural identifications in the tank (Reyes *et al.*, 2022) have shown that the water mass moving together with the tank (i.e. "impulsive mass") is roughly equal to the mass predicted with simplified tabulated values (Malhotra, Wenk and Wieland, 2000). Thus, the method of Malhotra, Wenk and Wieland (2000) will be used to determine the part of the mass that is moving together with the tank as well as the height that this should be attached.

Table 2 presents the summarized equivalent properties of the model. These properties were obtained considering an equivalent cylindrical tank of equivalent volume. Notice that the equivalent height in both principal directions is the same due to the radial symmetry of the tank. The height h_z for computing vertical reaction forces and the geometric P-delta effects is considered at half of the equivalent cylinder height. The total mass of the water (i.e., m_{water}=3,000kg) is considered in the vertical *z*-direction.

To compute the Rotational Inertia (RI) of the system around its center of mass, one would need to consider that the water neither rotates with the container as a rigid body nor it stays still. Thus, only a portion of this mass rotates. The accurate solution to this FSI problem is beyond the scope of this work. Therefore, the approximate equations given in (Partom, 1985; Raouf, 2005) are used for this specific geometry and yield an RI equal to 18% of solid volume RI. More information about the equivalent properties and how they were obtained can be found in (Reyes *et al.*, 2022).

Table 2. Summary of equivalent properties of the model.

Parameter expression	Value	Parameter expression	Value
m_{water}	*3,000 kg*	$m_z = m_{water} + m_{tank}$	*3,250 kg*
m_{tank}	*250 kg*	$h_x = h_y = \frac{h_{water}\ 0.77m_{water} + h_{tank}m_{tank}}{0.77m_{water} + m_{tank}}$	*1.804 m*
h_{water}	*1.829 m*	$h_z = \frac{h_{water}m_{water} + h_{tank}m_{tank}}{m_{water} + m_{tank}}$	*1.816 m*
h_{tank}	*1.573 m*	$I_x = I_y = I_x^{liquid} + I_x^{tank} = I_y^{liquid} + I_y^{tank}$	*373.6 kg-m²*
$m_x = m_y = 0.77 \cdot m_{water} + m_{tank}$	*2,560 kg*	$I_z = 0.05I_z^{liquid} + I_z^{tank}$	*203.3 kg-m*

1.3. Modeling the isolation device

The ISO3D-2G (Reyes and Almazán, 2020) device was used as an isolation device (see Figure 3b); however, any device that complies with the kinematic requirements of being vertically flexible and laterally rigid can be used with the VRI system. The ISO3D-2G device comprises an assembly of steel pieces and two types of high-damping rubber bearings: i) a central annular rubber that is deformed in compression, and ii) several rubber bands that are deformed in tension. The steel components create a kinematic mechanism that amplifies the deformation of the tensile rubber bands (Auad and Almazán, 2017). The vertical deformation of the device directly compresses the annular rubber, while it stretches the rubber bands in tension. The device can be modeled as a three DOF element: i) a vertical DOF associated only with compression forces F_z (the device is freely allowed to uplift), and ii) two coupled horizontal orthogonal DOFs associated with the lateral forces F_x and F_y. The device can be considered hinged at the top, since the moments transmitted by its rotation can be neglected.

The vertical behavior (F_z) is modeled with the Hyperelastic Bouc-Wen (HBW) model proposed by Reyes & Almazán (Reyes and Almazán, 2020; Reyes *et al.*, 2022). Since the compression and tensile rubber in the device has different kinematic contributions and deformation mechanisms, they were modeled separately. Figure 4 presents a manual fitting (choosing the parameters by visual inspection) of the model to each rubber contribution. This fitting was chosen to match medium and large deformation cycles; consequently, small deformation cycles are not well represented. The model can represent small and large deformation cycles simultaneously, but it would require a more sophisticated scheme for obtaining the material model parameters, such as stochastic optimization methods that achieve a good performance with complex hysteretic models with several parameters (Reyes *et al.*, 2022; Reyes *et al.*, 2023; Reyes, Katsamakas and Vassiliou, 2023). The horizontal Fx and Fy behavior is modeled with the nonlinear biaxial hysteretic model proposed by Park et al. (Park, Wen and Ang, 1986). This model was chosen to consider the simply supported condition of the device and the potential sliding between the devices and the ground. In this model the horizontal X and Y forces are coupled and given by $F_i = \mathbf{F_z}(u,Z)\mu Z_i$ (with $i=x,y$). $\mathbf{F_z}(u,Z)$ corresponds to the axial load of the device, μ is the friction coefficient between the surfaces in contact (μ=0.3 is adopted for the model), and Z_i *is the internal state variable*. The detailed equations of the HBW model and the parameters considered can be found in previous studies (Reyes and Almazán, 2020; Reyes *et al.*, 2022).

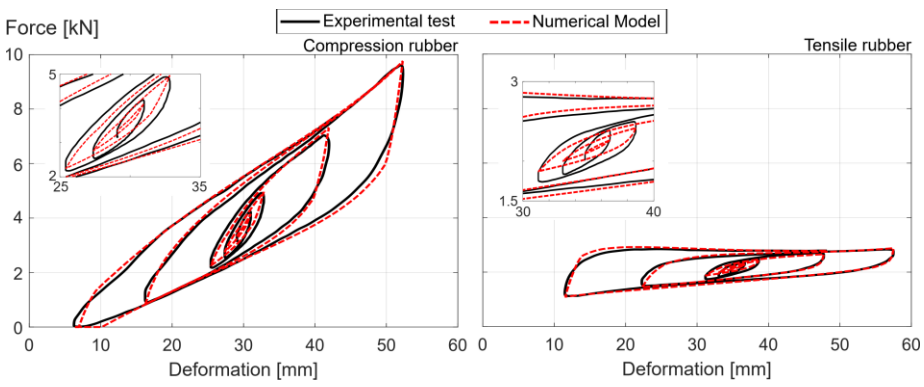

Figure 4. Numerical model calibration of the device.

5. Experimental and numerical results

After the 17 ground motions were applied, there was no visible damage in the tank or isolation devices. No sliding was observed, suggesting that the 2mm rubber pads that were placed under the isolation devices were enough to provide the necessary friction. In most of the ground motions, no significant uplift was recorded. However, ground motions #5, #11, and #17 did induce uplift, which remained smaller than 3mm in all cases and did not cause a noticeable increase of accelerations in the system due to drop-back impact.

Since there was not enough creep time for the devices under the weight of the tank, the excitations did cause a cumulative settlement of the tank. Figure 5a presents the accumulated vertical deformation on the devices after each test, including the initial filling and final water emptying. Note that the devices did not deform uniformly when filling the tank with water. This may be due to: a) the variability of the rubber mechanical properties in each device, and b) the induced mass eccentricity by the sloped bottom of the tank. The former seems to cause a small leaning of the tank toward devices 4 and 3, while the latter displaced the resultant vertical force almost 20 mm toward devices 1 and 4 (see plan layout on Figure 2), causing an additional smaller leaning towards this direction. This resulted in Device 4 being compressed approximately 5 mm more than Devices 1 and 2.

Figure 5b shows the time history of the measured vertical deformation on devices 1 and 3 subjected to the records #1 Talca-50% and #12 Synthetic-75%, with the latter having 50% larger PGA than the former. There is an accumulation of residual vertical deformation at the initial tests, stopping after test #6. For instance, the abrupt settlement in the intense part of record #1 (i.e., around the 25th second of the record) suggests that the vertical creep may be accelerated by large amplitude deformation cycles. This uneven settlement did not impact the system performance but caused a non-aesthetic leaning that may be relevant for possible stakeholders (e.g., wineries).

Figure 6 presents six outputs of interest obtained from the shaking table tests and numerical simulations for two of the records, selected due to the observed low and large displacement demand in each: #1 Talca-50% and #17 Synthetic-120%, respectively. The six outputs correspond to the measured (filtered) lateral accelerations (A_{bottom}, A_{top}), relative lateral displacements (D_{middle}, D_{top}), vertical deformation on device 1 ($D_{device\ 1}$), and rotation of the isolation interface (θ_{base}). For both records, a close-up is presented around the time instant when the maximum deformation occurred. In general, the displacement histories measured at the top and middle of the tank were in phase and proportional to the base rotation. This validates the rotation as a rigid body of the system. In terms of model prediction, It can be seen that the numerical model performs relatively better for a more intense record than for a weak one. This trend was observed in all records, and it is consistent with the chosen calibration of the model of the devices shown in Figure 4. Additionally, the model was able to capture well the low-frequency rocking mode and the high-frequency modes that source from the high (albeit not infinite) horizontal stiffness of the tank-leg / isolation-device assembly. Neglecting the convective mode of the tank seems to have no considerable negative effects on the performance of the model, further validating the used modeling approach for filled-to-the-top tanks of the considered aspect ratio. However, further studies are needed to extrapolate these conclusions and validate the proposed approach for tanks of different aspect ratios and shapes.

Figure 7 presents the relative errors obtained by the prediction of the observed peak responses in the records, together with their mean values. It arranges this data in scatterplots as a function of two intensity measures: PGA and peak ground velocity (PGV). In general, the error and the variability of the predictions are lower for more intense ground motions, irrespective of whether PGA or PGV are chosen as an intensity measure. There is no clear advantage in considering PGA or PGV as intensity measures. The error in predicting displacement was less than 30% in all but one cases. The error in predicting accelerations was in general less than 40%. These error values are comparable to other studies of isolation systems (Demetriades, Constantinou and Reinhorn, 1992) that did not include Fluid Structure Interaction. Moreover, in terms of average error, the displacements were predicted with a mean error of -1.2% and 7% for the displacements at the middle and the top of the tank, respectively. Total accelerations were underestimated with mean errors of -10.5% and -21.2% for the acceleration at the bottom and top of the mantle, respectively. This underestimation may be a consequence of neglecting higher modes resulting from the deformability of the structure since the errors obtained in the predicted acceleration in the top (Atop) were generally larger than those predicted in the middle

(Amid). This also can be observed in Figure 6, since the main difference in accelerations between the model and the tests are caused by a high-frequency oscillation.

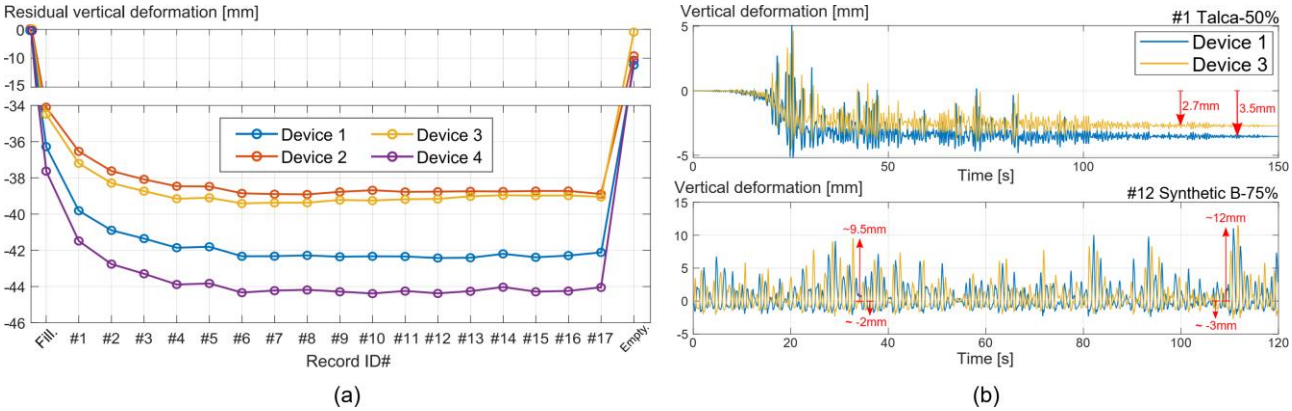

Figure 5. (a) Residual vertical deformation of the devices during the tests, and (b) time-history deformation of devices 1 and 3 for records #1 and #12.

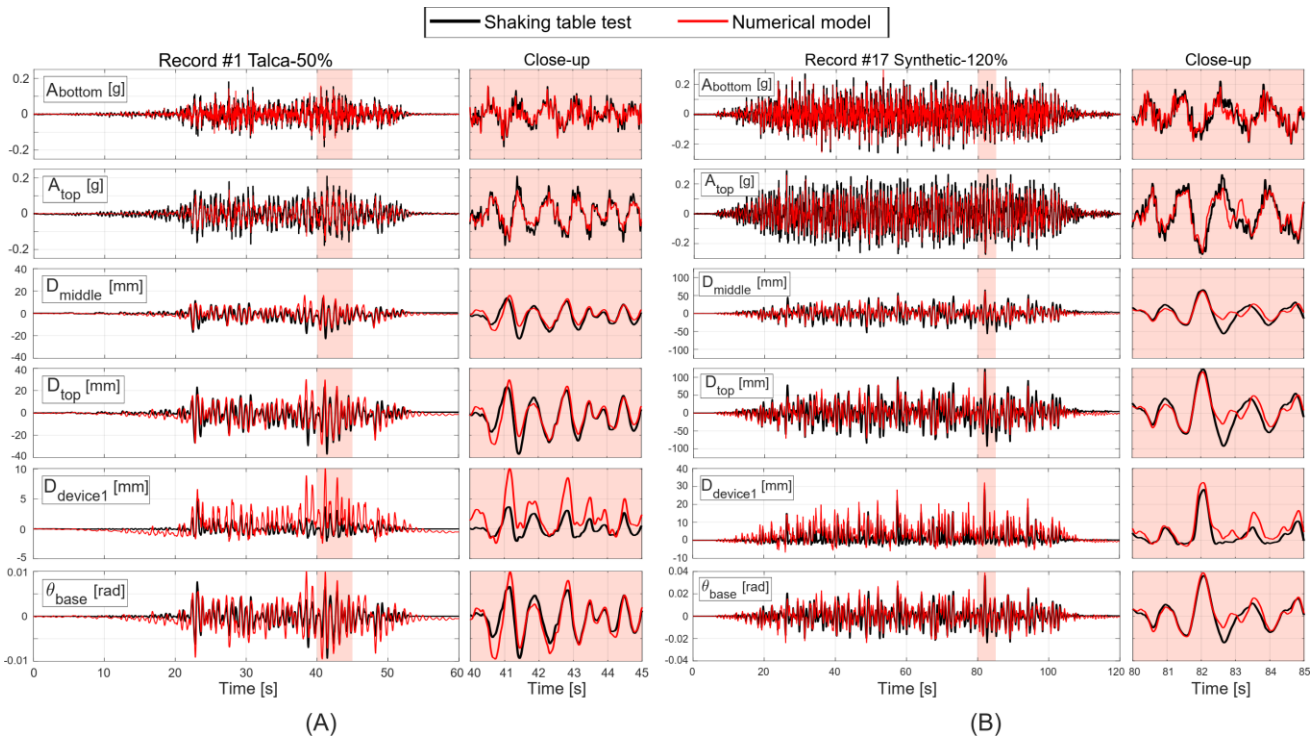

Figure 6. Prediction of the numerical model to: (a) record #1, and (b) record #17.

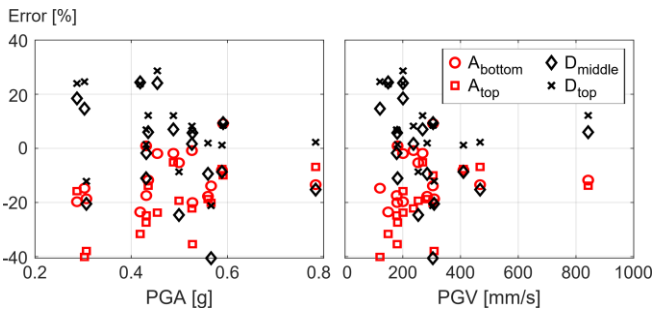

Figure 7. Error in the prediction of the peak responses.

6. Conclusions

In this work, the performance of a Vertical Rocking Isolation System based on unbonded rubber was experimentally analyzed via shake table tests. A 3000-liter capacity legged storage tank was supported on four ISO3D-2G devices to generate the vertical rocking isolation mechanism. The tank was subjected to 17 seismic records to evaluate its performance as an isolation system. A numerical model was developed to predict the observed behavior of the tank during the tests. The model considered a rigid superstructure supported on four nonlinear elements representing the isolation devices. The nonlinear force-deformation relation of the devices was represented using a hyperelastic Bouc-wen model. The liquid on the tank was modeled as an impulsive mass, neglecting convective terms.

During the seismic record tests, neither the tank nor the isolation devices exhibited any damage. The devices showed an initial settlement due to creep of the rubber; however, this phenomenon is quite limited and should not be a problem in practice. When emptying the water, the devices showed a residual deformation of nearly 10 mm. The tank presented a maximum top displacement of 124 mm, with a maximum total acceleration of approximately 0.19g, even for intense ground motions recorded during the 2010 M_w 8.8 Maule, Chile earthquake scaled by 1.2. This total acceleration of 0.33g could also be interpreted as the normalized base shear, which validates the effectiveness of the isolation system even for a relatively low isolation period (i.e., around 1 second).

The system's time history and peak responses were predicted relatively well with a simple yet detailed, rigid lumped-mass model. The maximum errors of peak response predictions were nearly less than 40%; however, they corresponded to specific records, and in general, all prediction errors remained below ±30%. In terms of mean errors, values of less than 10% and 21% were obtained for displacements and accelerations, respectively. These prediction errors are realistic and comparable to recent studies that perform analytical prediction of primary and secondary systems in seismically isolated structures (Demetriades, Constantinou and Reinhorn, 1992). Moreover, the model performed better for larger intensity seismic records, which are of interest in design.

The simplicity of the considered model for the tank is of great advantage for design; however, the assumptions and limitations need to be further studied and validated for tanks of different aspect ratios, shapes, and water levels. Finally, it is concluded that using vertically flexible devices at the base of some light structures to generate a rocking isolation mechanism effectively reduces the seismic demand on the structure, though the isolated modes and periods of the structure are shorter than 2.0 sec. Although there is no lateral translation at the base, the VRI system isolates the structure by allowing the lateral displacement of the CM.

7. Acknowledgments

This research has been supported by the Sawiris Foundation for Social Development with an ETH for Development grant, and by the following grants: ANID/FONDEF/VIU19E0130 “ISOVEP: Industrial Solutions for Operational Vibrations and Earthquake Protection”, ANID/FONDECYT/1201841 “Analysis, design and experimentation of solutions to mitigate the effects of impact forces on structures and equipment with two-dimensional and three-dimensional seismic isolation systems”, and ANID/FONDAP/15110017 “Research Center for Integrated Disaster Risk Management (CIGIDEN)”. The authors are grateful for the support.

8. References

Alessandri, S., Giannini, R., Paolacci, F., Amoretti, M. and Freddo, A. (2015) ‘Seismic retrofitting of an HV circuit breaker using base isolation with wire ropes. Part 2: Shaking-table test validation’, *Engineering Structures*, 98, pp. 263–274. Available at: https://doi.org/10.1016/j.engstruct.2015.03.031.

Almazan, J.L. and Reyes, S. (2021) ‘Device and system for three-dimensional vibration isolation’. Available at: https://doi.org/10.3929/ethz-b-000638580.

Auad, G.A. and Almazán, J.L. (2017) ‘Non linear vertical-rocking isolation system: Application to legged wine storage tanks’, *Engineering Structures*, 152, pp. 790–803. Available at: https://doi.org/10.1016/j.engstruct.2017.09.061.

Buckle, I.G. and Mayes, R.L. (1990) ‘Seismic Isolation: History, Application, and Performance—A World View’, *Earthquake Spectra*, 6(2), pp. 161–201. Available at: https://doi.org/10.1193/1.1585564.

Colombo, J.I. and Almazán, J.L. (2017) 'Experimental investigation on the seismic isolation for a legged wine storage tank', *Journal of Constructional Steel Research*, 133, pp. 167–180. Available at: https://doi.org/10.1016/j.jcsr.2017.02.013.

Daniell, J.E. and Schäfer, A.M. (2018) 'An analysis of wine industry impact and risk for earthquakes in Australia and globally: Part 1: Historical Impact Analysis, Exposure and Preliminary Results', *Australian Earthquake Engineering Society* [Preprint].

Demetriades, G.F., Constantinou, M.C. and Reinhorn, A.M. (1992) *Technical Report NCEER-92-0012: Study of Wire Rope Systems for Seismic Protection of Equipment in Buildings*, *Engineering Structures*. Buffalo, New York: Elsevier. Available at: https://doi.org/10.1016/0141-0296(93)90036-4.

Elmorsy, M. and Vassiliou, M.F. (2023) 'Effect of ground motion processing and filtering on the response of rocking structures', *Earthquake Engineering and Structural Dynamics*, 52(6), pp. 1704–1721. Available at: https://doi.org/10.1002/eqe.3837.

Goudarzi, M.A., Moosapoor, M. and Nikoomanesh, M.R. (2020) 'Seismic design loads of cylindrical liquid tanks with insufficient freeboard', *Earthquake Spectra*, 36(4), pp. 1844–1863. Available at: https://doi.org/10.1177/8755293020926191.

Housner, G.W. (1963) 'The behavior of inverted pendulum structures during earthquakes', *Bulletin of the Seismological Society of America*, 53(2), pp. 403–417. Available at: https://doi.org/10.1017/CBO9781107415324.004.

Kelly, T.E. (2008) *Development of Design Guidelines for rocking structures*. Holmes Consulting Group.

Makris, N. (2014) 'The role of the rotational inertia on the seismic resistance of free-standing rocking columns and articulated frames', *Bulletin of the Seismological Society of America*, 104(5), pp. 2226–2239. Available at: https://doi.org/10.1785/0120130064.

Makris, N. (2019) 'Seismic isolation: Early history', *Earthquake Engineering and Structural Dynamics*, 48(2), pp. 269–283. Available at: https://doi.org/10.1002/eqe.3124.

Makris, N. and Constantinou, M.C. (1992) 'Spring-viscous damper systems for combined seismic and vibration isolation', *Earthquake Engineering & Structural Dynamics*, 21(8), pp. 649–664. Available at: https://doi.org/10.1002/eqe.4290210801.

Malhotra, P.K., Wenk, T. and Wieland, M. (2000) 'Simple procedure for seismic analysis of liquid-storage tanks', *Structural Engineering International: Journal of the International Association for Bridge and Structural Engineering (IABSE)*, 10(3), pp. 197–201. Available at: https://doi.org/10.2749/101686600780481509.

McKevitt, W.E., Timler, P.A.M. and Lo, K.K. (1995) 'Nonstructural damage from the Northridge earthquake', *Canadian Journal of Civil Engineering*, 22(2), pp. 428–437. Available at: https://doi.org/10.1139/l95-051.

Moosapoor, M., Yousefi, M.M. and Goudarzi, M.A. (2019) 'An Experimental Study of Insufficient Free Board Effect on Fixed-Roof Cylindrical Tank Seismic Loads', *Journal of Seismology and Earthquake Engineering*, 21(3), pp. 13–30. Available at: https://iranjournals.nlai.ir/handle/123456789/775707 (Accessed: 20 July 2021).

Moreno, M., Colombo, J., Wilches, J., Reyes, S. and Almazán, J. (2023) 'Buckling of steel tanks under earthquake loading: Code provisions vs FEM comparison', *Journal of Constructional Steel Research*, 209, p. 108042. Available at: https://doi.org/10.1016/j.jcsr.2023.108042.

Olivares, C.I., de la Llera, J.C. and Poulos, A. (2020) 'Torsion control in structures isolated with the triple friction pendulum system', *Engineering Structures*, 216(May), p. 110503. Available at: https://doi.org/10.1016/j.engstruct.2020.110503.

Park, Y.J., Wen, Y.K. and Ang, A.H. (1986) 'Random vibration of hysteretic systems under bi-directional ground motions', *Earthquake Engineering & Structural Dynamics*, 14(4), pp. 543–557. Available at: https://doi.org/10.1002/eqe.4290140405.

Partom, I.S. (1985) 'Numerical calculation of equivalent moment of inertia for a fluid in a cylindrical container with partitions', *International Journal for Numerical Methods in Fluids*, 5(1), pp. 25–42. Available at: https://doi.org/10.1002/fld.1650050104.

Ramirez, V., Guzman Lucatero, E., Macias, J., Almazán, J.L. and Reyes, S.I. (2020) 'Analysis of the behavior of a flexible building with seismic isolation in various interfaces', *17 World Conference on Earthquake Engineering, Sendai, Japan*, 2408, pp. 2g – 0074. Available at: https://www.research-

collection.ethz.ch/handle/20.500.11850/638520.

Raouf A. Ibrahim (2005) *Liquid Sloshing Dynamics: Theory and Applications*, *Cambridge University Press*. Cambridge University Press. Available at: https://doi.org/10.1017/CBO9781107415324.004.

Reggiani Manzo, N. and Vassiliou, M.F. (2019) 'Displacement-based analysis and design of rocking structures', *Earthquake Engineering and Structural Dynamics*, 48(14), pp. 1613–1629. Available at: https://doi.org/10.1002/eqe.3217.

Reyes, S., Almazán, J.L., Colombo, J.I., Tapia, N. and de la Llera, J.C. (2020) 'Shaking Table Tests on Full-Scale Legged Liquid Storage Tanks Protected With a Vertical-Rocking Isolation System', *17 World Conference on Earthquake Engineering, Sendai, Japan*, 2408, p. C002408. Available at: https://www.researchgate.net/publication/345507107_Shaking_table_tests_on_full-scale_legged_liquid_storage_tanks_protected_with_a_vertical-rocking_isolation_system (Accessed: 5 July 2021).

Reyes, S.I., Vassiliou, M.F., Agathos, K. and Konstantinidis, D. (2022) 'Effects of two testing protocols on the material model parameter identification for rubber-like materials', in *Proceedings of the Third European Conference on Earthquake Engineering and Seismology – 3ECEES*. Romania: Editura Conspress, pp. 2359–2367. Available at: https://doi.org/10.3929/ethz-b-000571690.

Reyes, S.I., Almazán, J.L., Vassiliou, M.F., Tapia, N.F., Colombo, J.I. and de la Llera, J.C. (2022) 'Full-scale shaking table test and numerical modeling of a 3000-liter legged storage tank isolated with a vertical rocking isolation system', *Earthquake Engineering and Structural Dynamics*, 51(6), pp. 1563–1585. Available at: https://doi.org/10.1002/eqe.3628.

Reyes, S.I., Vassiliou, M.F., Agathos, K. and Konstantinidis, D. (2023) 'Finite Element Modeling of the Rolling Behavior of a Polyurethane Sphere for Low-Cost Seismic Isolation Applications', in *COMPDYN Proceedings*. Eccomas Proceedia. Available at: https://doi.org/doi.org/10.3929/ethz-b-000615832.

Reyes, S.I. and Almazán, J.L. (2019) *A three-dimensional isolation system with uplift allowed for industrial structures*, *Congreso Chileno de Sismología e Ingeniería Sísmica*. Available at: https://www.researchgate.net/publication/345507774_A_three-dimensional_isolation_system_with_uplift_allowed_for_industrial_structures (Accessed: 5 July 2021).

Reyes, S.I. and Almazán, J.L. (2020) 'A novel device for a vertical rocking isolation system with uplift allowed for industrial equipment and structures', *Engineering Structures*, 214, p. 110595. Available at: https://doi.org/10.1016/j.engstruct.2020.110595.

Reyes, S.I., Katsamakas, A.A. and Vassiliou, M.F. (2023) 'Vibration isolation capabilities of a low-cost seismic isolation system based on elastomeric rolling spheres for masonry structures', in *Proceedings of the International Conference on Structural Analysis of Historical Constructions (SAHC)*.

Riley, M., Stark, C., Kempner, L. and Mueller, W. (2006) 'Seismic Retrofit Using Spring Damper Devices on High-Voltage Equipment Stands', *Earthquake Spectra*, 22(3), pp. 733–753. Available at: https://doi.org/10.1193/1.2216736.

Rosewitz, J. and Kahanek, C. (2014) 'Performance of Wine Storage Tanks : Lessons From the Earthquakes Near Marlborough', in *Insitute of stuctural engineers*.

Tapia, N.F., Almazán, J.L., Valdebenito, N. and Reyes, S.I. (2023) 'Experimental validation of an energy-dissipating anchoring system for continuously-supported storage tanks', in *Structures*, pp. 2324–2340. Available at: https://doi.org/10.1016/j.istruc.2023.07.039.

Wada, A., Kani, N., Hirano, S., Kamikouchi, H. and Kimura, M. (2008) 'Seismic Isolated Structures Applied to from Detached Houses to High-rise Apartments in Japan', in *5th International conference on urban earthquake engineering*.

Wang, L. and Ishihara, T. (2020) 'A study of the effects of foundation uplift on the seismic loading of wind turbine tower and shallow foundation using a new dynamic Winkler model', *Engineering Structures*, 219. Available at: https://doi.org/10.1016/j.engstruct.2020.110745.

Zhang, Z. and Zhou, Y. (2023) 'Experimental and analytical investigations on horizontal behavior of full-scale thick rubber bearings', *Soil Dynamics and Earthquake Engineering*, 174, p. 108202. Available at: https://doi.org/10.1016/j.soildyn.2023.108202.